RSC Advances

PAPER

View Article Online
View Journal | View Issue

Cite this: *RSC Adv.*, 2021, **11**, 28286

Geometry transformation of ionic surfactants and adsorption behavior on water/*n*-decane-interface: calculation by molecular dynamics simulation and DFT study†

Wannian Zhang,‡[abc] Ming-Yuan Zhang,‡[c] Kai Wang,[bc] Ruixia Sun,[c] Shanlin Zhao,[ac] Zhiqiang Zhang,*[a] Yu-Peng He *[abc] and Fang Yu *[bc]

Understanding the effect of surfactant structure on their ability to modify interfacial properties is of great scientific and industrial interest. In this work, we have synthesized four amide based ionic surfactants under acidic or basic conditions, including **CTHA·HCl**, **CTEA·HCl**, **CTHA$^-$Na$^+$** and **CTEA$^-$Na$^+$**. Experiments have proved that the anionic surfactant with polyethylene oxide groups (**CTEA$^-$Na$^+$**) had the lowest surface tension on the water/*n*-decane interface. Molecular dynamics simulations have been applied to investigate the structural effect on the adsorption behavior of four different surfactants. The surface tension, interface thickness, interface formation energy, density profiles, order parameters, radial distribution function on the water/*n*-decane interfaces were calculated and compared. During the equilibrium states, we found that the interface configuration of two cationic surfactants are almost linear while the two anionic surfactants are changed to bending shapes due to the different positions of the hydrophilic head groups. Further DFT study and wavefunction analysis of surfactants have shown that **CTEA$^-$Na$^+$** can form stronger vdW interactions with *n*-decane molecules due to a more neutral electrostatic potential distribution. Meanwhile, the introduction of polyethylene oxide groups has offered more H-bonding sites and resulted in more concentrated H-bonding interactions with water molecules. The difference of weak interactions may contribute to the conformational change and finally affect the interface properties of these ionic surfactants.

Received 16th June 2021
Accepted 15th August 2021

DOI: 10.1039/d1ra04669a

rsc.li/rsc-advances

Introduction

Amide based ionic surfactants,[1] typically consisting of both amide bond and acidic or basic groups as hydrophilic moieties, have gained substantial interest during the past decades. Their amphiphilicity enables these amide based surfactants to adsorb on the interface and significantly reduce the interfacial tension. Due to the unique structural feature and interfacial properties, amide based ionic surfactants are widely used in daily life and industrial processes, including detergents, food and cosmetics, and especially in large-scale operations of oil extraction[2] as oil displacement agents.

Recently, due to the wide application of amide ionic surfactants in oilfield chemistry, research about structural influence on the related absorption behavior on water/*n*-decane interface to mimic a simplified oil environment has received substantial attentions.[3] Molecular design and synthesis have a significant influence on absorption behavior of amide based ionic surfactants,[4] including changing the type and position of hydrophilic heads or the component and length of hydrophobic tails.[5] Moreover, adjusting pH value could obtain both cationic and anionic surfactant due to the structural feature of amide based ionic surfactants.[6] However, investigation of the structural effect on interfacial properties of amide based ionic surfactants on water/*n*-decane interface is limited. Especially, research about interpretation the weak interactions between the ionic surfactants, oil phase and water molecules at a quantum level is extremely limited.

Recent elegant computational works have confirmed that molecular dynamics (MD) simulation is an effective tool to probe the adsorption behavior of surfactant[7] on oil/water

[a]*Key Laboratory for Functional Material, Educational Department of Liaoning Province, School of Chemical Engineering, University of Science and Technology Liaoning, Anshan 114051, P. R. China. E-mail: zzq@ustl.edu.cn; yupeng.he@lnpu.edu.cn*

[b]*State Key Laboratory of Fine Chemicals, Ningbo Institute of Dalian University of Technology, No. 26 Yucai Road, Jiangbei District, Ningbo, 315016, P. R. China. E-mail: fang.yu@lnpu.edu.cn*

[c]*Key Laboratory of Petrochemical Catalytic Science and Technology, Liaoning Petrochemical University, Dandong Lu West 1, Fushun 113001, Liaoning, P. R. China. Tel: +86-2456860548*

† Electronic supplementary information (ESI) available: Detailed experimental procedures and spectroscopic data of all new compounds. See DOI: 10.1039/d1ra04669a

‡ W. Zhang and M.-Y. Zhang contributed equally.

interfaces. Ding group studied the structural influence of sulfobetaine-type ionic surfactant to the water/*n*-decane interface.[8] Shiling Yuan and co-workers have studied that when the attaching position of benzenesulphonate group has shifted from one side to the middle of the dodecyl chain of SDBS, the molecular aggregation behaviors have been dramatically changed.[9] Despite these pioneering works, however, limited research has given deeper interpretation about the weak interactions between the ionic surfactants and oil environment the quantum level.

In this work, based on our previous research,[4f] we initially synthesized **CTHA** as an ionic surfactant. We then introduced polyethylene oxide groups to the hydrophobic tail and obtained **CTEA**. As a result, two cationic surfactants **CTHA·HCl**, **CTEA·HCl**, and then two anionic surfactants **CTHA$^-$Na$^+$**, **CTEA$^-$Na$^+$** were formed by treatment of NaOH. The surface tension of these four surfactants was measured. Subsequently, molecular dynamics simulation at the water/*n*-decane interface was utilized for shedding light to the relationship between monomer geometry of ionic surfactants and their interfacial behavior. Next, conformational and dynamical properties of surfactant molecules were evaluated by the analysis of the molecular orientation, the interfacial formation energy, and the thickness of the system. In addition, in order to study the effect of polyethylene oxide groups in the carbohydrate chain, the radial distribution function (RDF) was measured between the hydrophilic ion head groups and water. Finally, further DFT study[10] and wavefunction analysis of surfactants have offered a more fundamental study of weak interactions, including contribution and distribution of electrostatic and dispersion action.

Results and discussion

Synthesis

Four different surfactant molecules were designed and synthesized (Scheme 1). First, decylsuccinic anhydride underwent ring-opening reaction with Boc-protected diamine and glycol included diamine to obtain *N*-acetyl carboxylic acids **CTHA·HCl** and **CHEA·HCl** (at this time, the carboxyl group was not protonated). Then these cationic structures were converted to anionic molecules by treatment with NaOH and the carboxyl group was protonated to form sodium salts. The whole synthetic route featured a high yield and a mild condition under room temperature (detailed information see ESI†). The ionic structures differed in the polarity and position of the head groups as well as the component of the alkyl chain.

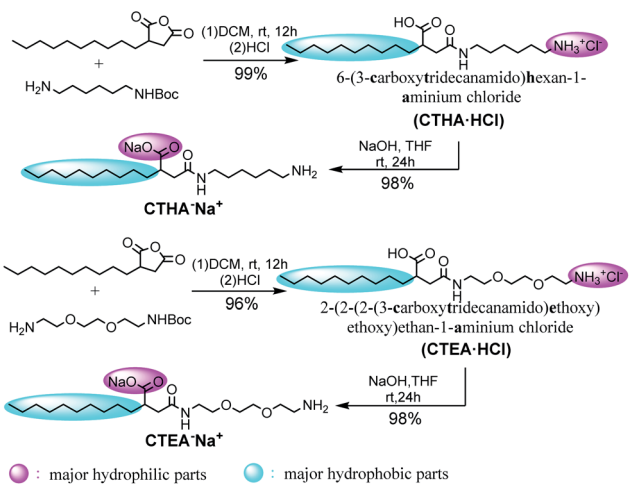

Scheme 1 Synthetic route of ionic structures.

Equilibrated system: surfactant conformation

Snapshot of simulated **CTHA·HCl** monolayer was shown in Fig. 1. The water phase was in the middle and the *n*-decane phases were on both sides. All surfactants stayed at the interfaces, and none of them diffused into the bulk phases and alkyl chains were randomly oriented in monolayer systems during the whole simulation processes (all the equilibrium states of MD simulation are shown in the Fig. S3† and all the RMSD of MD simulation are shown in the Fig. S4.†). Direct contact between oil and water phases were still observed. The *n*-decane solvated the surfactant tails and prevented them from aggregating together. Monomolecular configurations of four surfactants at the equilibrium states were extracted and shown in Fig. 2. The extracted individual molecular configurations of four surfactants at the interface were altered with different pH values. The hydrophilic group of **CTHA·HCl** and **CTEA·HCl** anionic surfactants located at the terminal of the molecules, and the configurations were almost stretched to a liner shape. In contrast, the hydrophilic groups of **CTHA$^-$Na$^+$** and **CTEA$^-$Na$^+$** salts were in the middle of the main chain and the configurations were bent to a bending shape, while the hydrophobic alkyl chain went deeply into the oil phase.

Interfacial tension

The interfacial tension (γ_{sim}) was calculated according to the Kirkwood–Buff theory.[11]

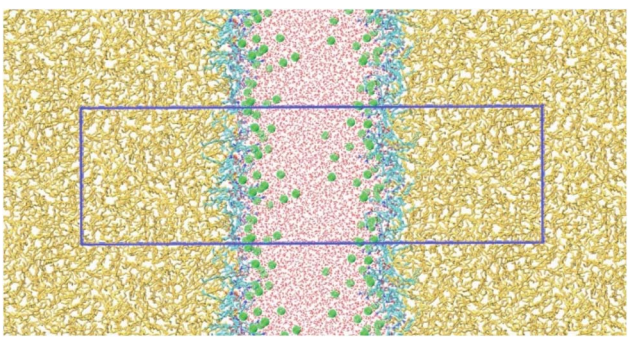

Fig. 1 Snapshot of the simulated CTHA·HCl monolayer system at the water/*n*-decane interface. The surfactant molecules are represented with thick licorice lines, and some hydrogen atoms in the surfactant and *n*-decane molecules are not shown for clarity. Periodic images are also shown, and the blue lines represent the system borders in our simulations.

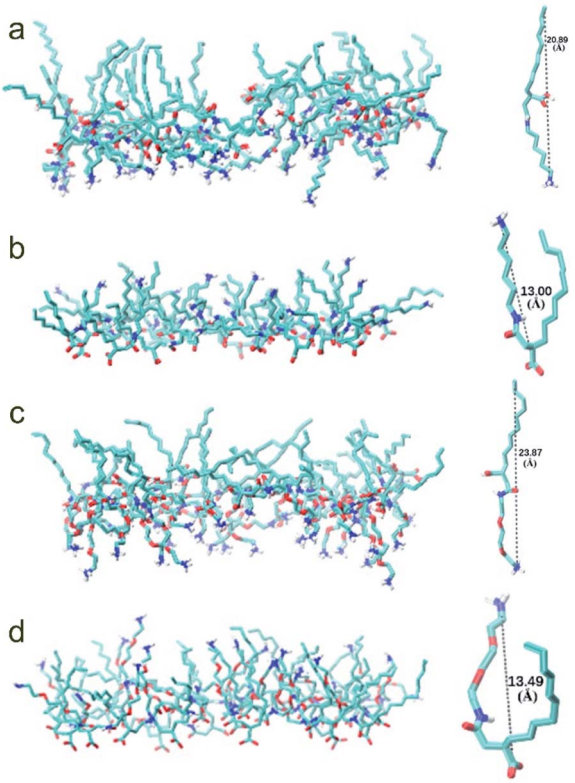

Fig. 2 The monomolecular layer structures and configurations. (a) CTHA·HCl surfactant (b) $CTHA^{-}Na^{+}$ surfactant (c) CTEA·HCl surfactant (d) $CTEA^{-}Na^{+}$ surfactant. For visual clarity, all the nonpolar hydrogen atoms were not displayed. The structure of surfactant was displayed with the VMD software.

$$\gamma_{sim}(t) = \frac{1}{n}\int_0^{L_z}\left[P_{zz}(z,t) - \frac{P_{xx}(z,t)+P_{yy}(z,t)}{2}\right]dz \quad (1)$$

where $P_{\alpha\alpha}$ ($\alpha = x, y, z$) is the diagonal components of the pressure tensor, L_z is the box length in the z axis direction, and n is the number of interfaces in the system ($n = 2$).

The interfacial tension of the bare water/*n*-decane interface was calculated to be 51.4 mN m^{-1}, which corresponded perfectly with the experimental value of 51.7 mN m^{-1},[12] and the interfacial tension γ_{sim} of the monolayer systems also agreed well with the experimental values at similar temperatures at the critical micelle concentration (CMC) γ_{cmc} (see ESI Table S1†). The critical surface tension of the anionic surfactants ($CTHA^{-}Na^{+}$ and $CTEA^{-}Na^{+}$) was lower than that of the cationic surfactants (**CTHA·HCl** and **CTEA·HCl**). Secondly, the surfactant $CTEA^{-}Na^{+}$ surfactant with polyethylene oxide groups has the lowest surface tension (experimental γ_{cmc} = 25.2 mN m^{-1} and calculated 26.4 mN m^{-1}).

Interface formation energy

To compare the energetic stability of each system, the interface formation energy (IFE) was defined and calculated as follows:

$$\mathrm{IFE} = \frac{E_{total} - \left(nE_{surfactant,single} + E_{decane-water}\right)}{n} \quad (2)$$

The value of IFE is a measure of the average intermolecular interaction per surfactant molecule arising from the insertion of one surfactant molecule into the *n*-decane–water interface. E_{total} denoted the energies of the whole system. $E_{surfactant,single}$ was calculated from a separate 5 ns MD simulation in vacuum at the same temperature of every single surfactant. $E_{decane-water}$ was also calculated at the same temperature for 5 ns (Fig. 3).

Calculated IFE was summarized in Table 1. It can be seen from the table that the E_{total}, $E_{surfactant,single}$ of $CTEA^{-}Na^{+}$ surfactants and IFE were the lowest, which means that the $CTEA^{-}Na^{+}$-mediated interface was the most stable in terms of energy.

Density profiles

Density profiles along the z axis are shown in Fig. 4. It should be noted that the densities of each phase in the *n*-decane–surfactant–water system (black line, 0.723 ± 0.005 g cm^{-3} for *n*-decane and red line, 0.994 ± 0.005 g cm^{-3} for water) agreed well with those of the pure bulk phase (0.725 g cm^{-3} for *n*-decane[13] and 0.997 g cm^{-3} for water).[14] This showed that the simulation was sufficiently large enough to study a realistic interface between two bulk phases. Most of the ions stay between the water and the surfactant monolayer during simulation time and the Na^{+}/Cl^{-} ions (green line) bound to ionic head-groups (orange line) at the interface.

Interfacial thickness

To further characterize the interface, we have calculated the interfacial thickness as shown in Table 2. Then, we defined the thickness as the distance between the two positions where the densities of the *n*-decane and water phases are at 90% of their respective bulk densities obtained from the density profiles.[15] The thickness of the top and bottom interfaces were measured independently, and the reported thickness is an average thickness of the top and bottom.

For the bare *n*-decane-water interface (in the absence of surfactants), the interfacial thickness was determined to be 4.10 Å, which was in good agreement with the measured thickness

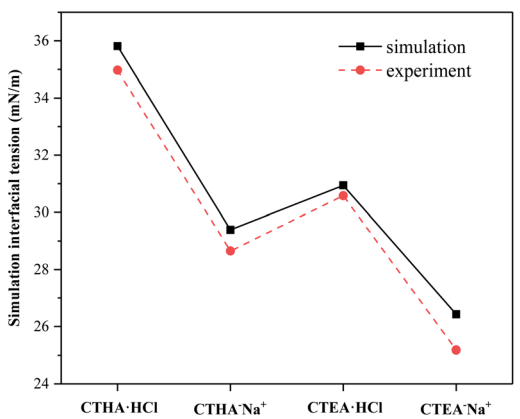

Fig. 3 Comparison of interfacial tension between our simulation and the experiment.

Table 1 Interface formation energy of surfactants

System	E_{total}[a] (kJ mol^{-1})	$E_{surfactant,single}$[b] (kJ mol^{-1})	IFE[c] (kJ mol^{-1})
CTHA·HCl	−183 523	−386.098	−232.318
CTHA$^-$Na$^+$	−188 001	−403.245	−285.149
CTEA·HCl	−185 277	−396.63	−251.02
CTEA$^-$Na$^+$	−190 153	−443.767	−289.805

[a] The energy of whole system. The energy of bare *n*-decane–water system. $E_{decane-water}$: −146 418 kJ mol^{-1}. [b] The energy of single surfactant molecule. [c] Interface formation energy (IFE), the cross-sectional area is 5 × 5 nm^2, IFE data is derived from the average of all equilibrium states.

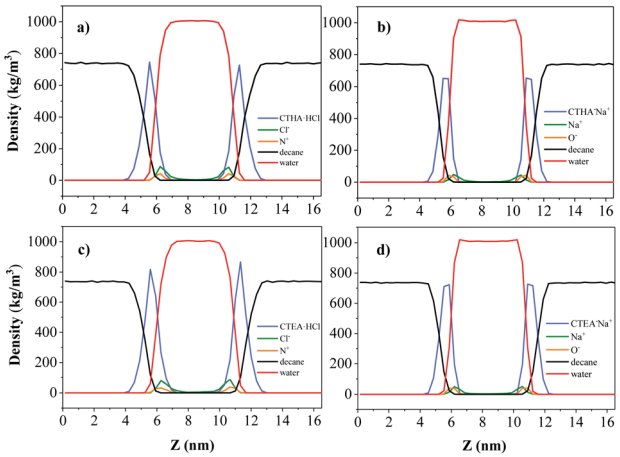

Fig. 4 Density profiles along the *z* axis: *n*-decane (black), water (red), Na^+/Cl^- ions (green), N^+/O^- ions (orange) for (from left to right) (a) **CTHA·HCl**, (b) **CTHA$^-$Na$^+$**, (c) **CTEA·HCl** and (d) **CTEA$^-$Na$^+$**.

Table 2 Interfacial thickness

System	t_i[a] (nm)		t_{total}[b] (nm)	L_z[c] (nm)
n-Decane–water	*n*-Decane	0.33	0.41	15.004
	Water	0.38		
CTHA·HCl	*n*-Decane	1.16	1.71	16.860
	Water	0.74		
CTHA$^-$Na$^+$	*n*-Decane	0.82	1.47	16.814
	Water	0.50		
CTEA·HCl	*n*-Decane	1.10	1.72	16.878
	Water	0.79		
CTEA$^-$Na$^+$	*n*-Decane	0.85	1.50	16.842
	Water	0.53		

[a] i = oil or water. t_{oil} and t_{water} are defined as the 10–90 thickness of the *n*-decane and water phases, respectively. [b] t_{total} are defined as the 90–90 thickness of the *n*-decane and water phases. [c] L_z: height of the box.

(4.6 ± 0.2 Å) observed from the reported synchrotron X-ray reflectivity experiment.[12]

From the results in Table 2, it was clear that the interfaces thickness (t_i) of water/*n*-decane were broadened with the addition of a surfactant because *n*-decane and water penetrated hydrophobic alkyl tails and polar groups, respectively. Interestingly, this interface broadening occurred mainly in the *n*-decane side and was strongly dependent on the attachment position of hydrophilic groups in the surfactant backbones. When the attaching positions shifting form one side to the middle of molecules, configurations of individual molecules at the interface dramatically changed from linear to bending shape. It can be seen that interface thickness (t_{total}) and box height (L_z) of **CTHA·HCl** and **CTEA·HCl** were both thicker and higher than those of **CTHA$^-$Na$^+$** and **CTEA$^-$Na$^+$**. By comparing anionic surfactants (**CTHA$^-$Na$^+$** and **CTEA$^-$Na$^+$**), we found that thicker thickness of the interface matched with lower the interfacial tension. Moreover, after careful observation, surfactant molecules with the addition of polyethylene oxide groups (**CTEA·HCl** and **CTEA$^-$Na$^+$**) had thicker interface for t_{total} due to the better miscibility in the oil and water phases.

Order parameter

A previous simulation study[4a] found that when the monomer structure was similar to each other, the changing trend of the surface tension was contrary to that for order parameter. Calculation of order parameters for surfactants could be used to evaluate its capacity in the reduction of surface tension. To analyze the conformation of the surfactant molecules in the monolayer, we have calculated the order parameter for the 10 terminal carbons of the primary alkyl chain. These 10 carbons represent the effective length of the surfactant tail. The order parameter is given by

$$S_z = \frac{3}{2}\langle \cos^2 \theta_z \rangle - \frac{1}{2} \quad (3)$$

where θ_z is defined as the angle between the vector formed by the first and last carbon of the ten carbon chain and the normal axis to the interface. Based on this definition, the chains are disordered when $S_z = 0$, horizontally aligned when $S_z = -0.5$, and vertically aligned when $S_z = 1$.

S_z, for all four surfactants was given in Fig. 5. The detailed information on how each tail atom was oriented could be seen from the average order parameters of each atom with the same index. The S_z of each atom for all surfactants decreased monotonically from near the interface to the far end of the tails from 1–10. The order of the vectors contacting the water phase was governed by the head group, they tended to interact with as many water molecules as possible to make the system more stable, so the vector value closer to the ion head group was higher (such as 1–3). Furthermore, the **CTHA$^-$Na$^+$** and **CTEA$^-$Na$^+$** tail chains were closer to the hydrophilic head groups, so the S_z value is higher (green and black line). The

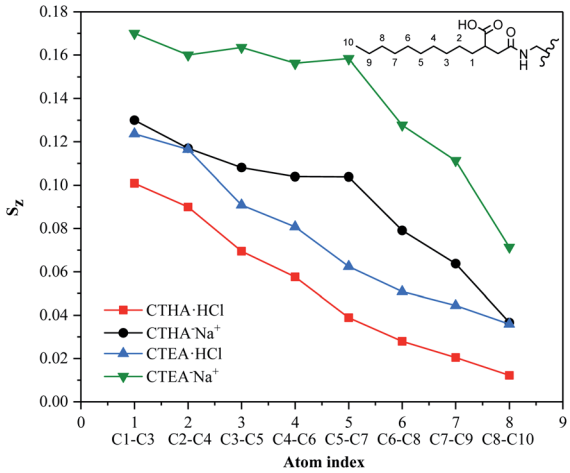

Fig. 5 Order parameter of the surfactant tail S_z comprising of the 10 terminal carbons. The alkane chain has 10 carbon atoms, and the 8 values in the figure correspond to C1–C3, C2–C4, C3–C5, C4–C6, C5–C7, C6–C8, C7–C9, C8–C10.

decrease of S_z indicated the surfactants were flexible and random in orientation.

Head group solvation

The structure of liquids can often be well characterized by the radial distribution function (RDF) of atomic density.

$$g_{AB}(r) = \langle \rho_B(r) \rangle / \langle \rho_B \rangle_{local} \quad (4)$$

which represents the probability of finding particle B within the range $r + dr$ around particle A. The solvation of surfactant ion-head groups had been investigated by RDF. Fig. 6 shown the radial distribution function of the water oxygen (OW) atom for the oxygen/nitrogen (O^-/N^+) atom for surfactants.

In Fig. 6a, the peak heights of different surfactants and different concentrations were basically the same. However, at the peak position, the N^+-OW RDF of **CTHA·HCl** and **CTEA·HCl** (red line and blue line) showed one large peak at 0.28 nm with a much smaller second peak at 0.49 nm, indicating the locations of the first and second solvation shell of the surfactant head groups, and a small third peak can be observed at around 0.65 nm. The first and second solvated shells of the O^--OW RDF for **CTHA⁻Na⁺** and **CTEA⁻Na⁺** (black line and green line) anionic surfactants were around 0.26 nm and 0.49 nm, respectively. Similarly, a small third peak could be observed at about 0.7 nm. As can be seen from Fig. 6b, the hydrophilic ion head group of **CTHA⁻Na⁺** and **CTEA⁻Na⁺** (black line and green line) was much closer to the oxygen atom in water, and the stronger the hydrogen bond could be formed.

Number of hydrogen bonds

To compare the hydrophilicity of the four surfactants, the number of hydrogen bonds formed in the entire trajectories of the four systems was calculated (Fig. 7). The hydrogen bond geometry criterion we use defaults to R–A (3.5 Å to 30°).[16] The number of hydrogen bonds between the two anionic surfactants and water was far greater than that between the two cationic surfactants and water (green and black line *vs.* blue and red line), which matched well with RDF data. However, as seen from anionic surfactants, **CTEA⁻Na⁺** molecules also had more hydrogen bonds with water than **CTHA⁻Na⁺** molecules due to the polyethylene oxide groups.

DFT study and wavefunction analysis

Considering the structural modification of the hydrophilic groups and the different interface properties of the four surfactant molecules, it is meaningful to analyze the electrostatic potential (ESP) distribution (Fig. 8). ESP is a result of wavefunction analysis at a quantum level and could further display the details of dispersion and electrostatic interactions of surfactant molecules, offering crucial information to understand the weak interactions. In all the four ionic surfactants, the

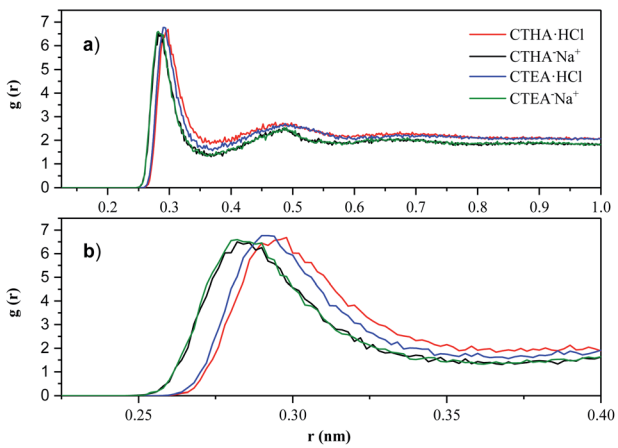

Fig. 6 (a) N^+-OW RDF of **CTHA·HCl** and **CTEA·HCl** (red line and blue line); O^--OW RDF of **CTHA⁻Na⁺** and **CTEA⁻Na⁺** (black line and green line). (b) Magnified image of the first peak of (a).

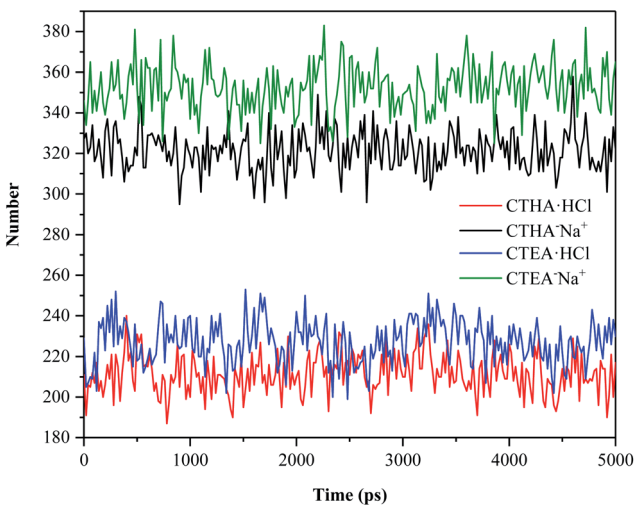

Fig. 7 Number of hydrogen bonds.

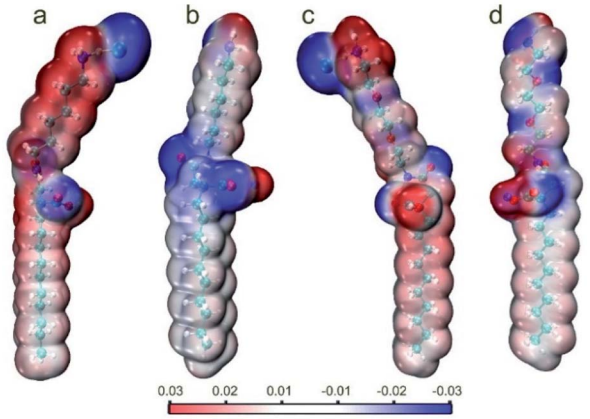

Fig. 8 Electrostatic potential (ESP) distribution of (a) CTHA·HCl, (b) $CTHA^{-}Na^{+}$ (c) CTEA·HCl, and (d) $CTEA^{-}Na^{+}$.

blue region is strongly negative while (amide group, ammonium salt, carboxylic acid and counter ion Cl^{-}) the red region is strongly positive (H^{+} and counter ion Na^{+}). Except these counter ions, sites that can act as H-bond donors and/or acceptors in the surfactant molecules were clearly exhibited. Moreover, the introduction of polyethylene oxide groups enhanced the negative potential of the hydrophilic group and resulted in more hydrogen bonding sites, which can form more density H-bonding interactions on the interface (Fig. 8c and d). In Fig. 8b and d (**$CTHA^{-}Na^{+}$/$CTEA^{-}Na^{+}$**), the ESP of the hydrophobic chains of the two anionic surfactants tends to be zero and is more neutral than cationic surfactants in Fig. 8a and c. Usually, neutral ESP is considered to be the dominant role of van der Waals effect of hydrocarbon chains, including dispersion and exchange- repulsion potential.[7d] Therefore, **$CTHA^{-}Na^{+}$/$CTEA^{-}Na^{+}$** can better interact with *n*-decane through van der Waals than **CTHA·HCl** and **CTEA·HCl** (Fig. 8a and c).

In order to better illustrate relationship between weak interactions and the adsorption conformation from a more microscopic respect, one target surfactant and other molecules within 5 Å (including water molecules, *n*-decane molecules and other surfactant molecules) during the MD equilibrium state were chosen as the research object and weak interactions were investigated by Multiwfn 3.8, mainly including H-bonding and vdW interactions.

It was clear from Fig. 9a and d, the conformation of cyan molecules was dramatically changed from an amine salt to a carboxylic sodium. The **$CTEA^{-}Na^{+}$** was curved while **CTEA·HCl** presented relatively a linear conformation. Also, there were more *n*-decane molecules (gray) in the **$CTEA^{-}Na^{+}$** system due to the more neutral ESP. Fig. 9b and e were magnified images of Fig. 9a and d. It was clear that introduction of polyethylene oxide groups made **$CTEA^{-}Na^{+}$** form more H-bonds network with water. The water molecules surrounded more tightly with the central **$CTEA^{-}Na^{+}$** and the thickness of the water layer is smaller. When we hided all the molecules in Fig. 9c and f, weak interactions were more obviously shown as green and blue plates (the green plates mainly stand for vdW interactions while blue plates mainly stand for H-bonding interactions). **$CTEA^{-}Na^{+}$** has a more neutral ESP than **CTEA·HCl**, therefore there are much stronger vdW interactions with *n*-decane molecules (green plates) in Fig. 9f than 9c. Introduction of the polyoxyethyl ether units has offered more H-bonding sites and there are more H-bonding interactions (blue plates) in Fig. 9f than 9c and these H-bonds dragged the chain with polyoxyethyl ether lay down toward the water phase. These differences in weak interactions may mainly contribute the conformational change of surfactants, which finally affected the properties of the interface.

Experimental

Materials

All organic solvents and reaction reagents were analytical grade and purchased from Inno-Chem GmbH. All reagents were used as received without further purification. The water used in the current study was of Millipore Milli-Q grade.

Surfactant aqueous preparation

Four surfactants aqueous solutions with different concentrations were prepared by dispersing surfactant samples in water (Millipore) by sonication. The aqueous solutions were all homogeneous and clear at 25 °C.

Equilibrium surface tension

The equilibrium surface tension was determined with the platinum ring method by using JK99B (Shanghai Zhongchen Digital Technic Apparatus Co., Ltd.). The maximum uncertainty on γ values is ± 0.05 mN m^{-1}. All the measurements were performed at 25.0 ± 0.1 °C and repeated at least three times to obtain the average value.

Surfactant model

The water/*n*-decane simulation model consisted of an intermediate layer of water and two layers of *n*-decane on both sides. Table 3 listed information for constructing the studied models, including the number of surfactants per surfactant N_{sur}, the area per surfactant A_s. Surfactant molecules and *n*-decane molecules were optimized earlier with the ATB (version 3.0).[18] After geometry optimization, Packmol program was utilized to include the listed molecules into the simulation model.[19] The surfactants are initially aligned perpendicular and distributed at both sides of the equilibrated water cell with their head groups in the vicinity of the water layer. In order to keep the charge neutral, sodium or chloride ions were randomly inserted into the water, according to the default rules to achieve a reasonable protonation state by GROMACS. Periodic boundary conditions were implemented for all *xyz* directions. The initial simulation box for the oil–water–surfactant system measured around $5 \times 5 \times 17$ nm^3. The *x* and *y* dimensions (~5 nm) of the systems were kept constant to maintain stable interfaces, leaving the *z* dimension (~17 nm) adjustable for an appropriate pressure. Energy minimization was performed to remove any overlaps with a time step of 5.0 fs, $F_{max} \leq$

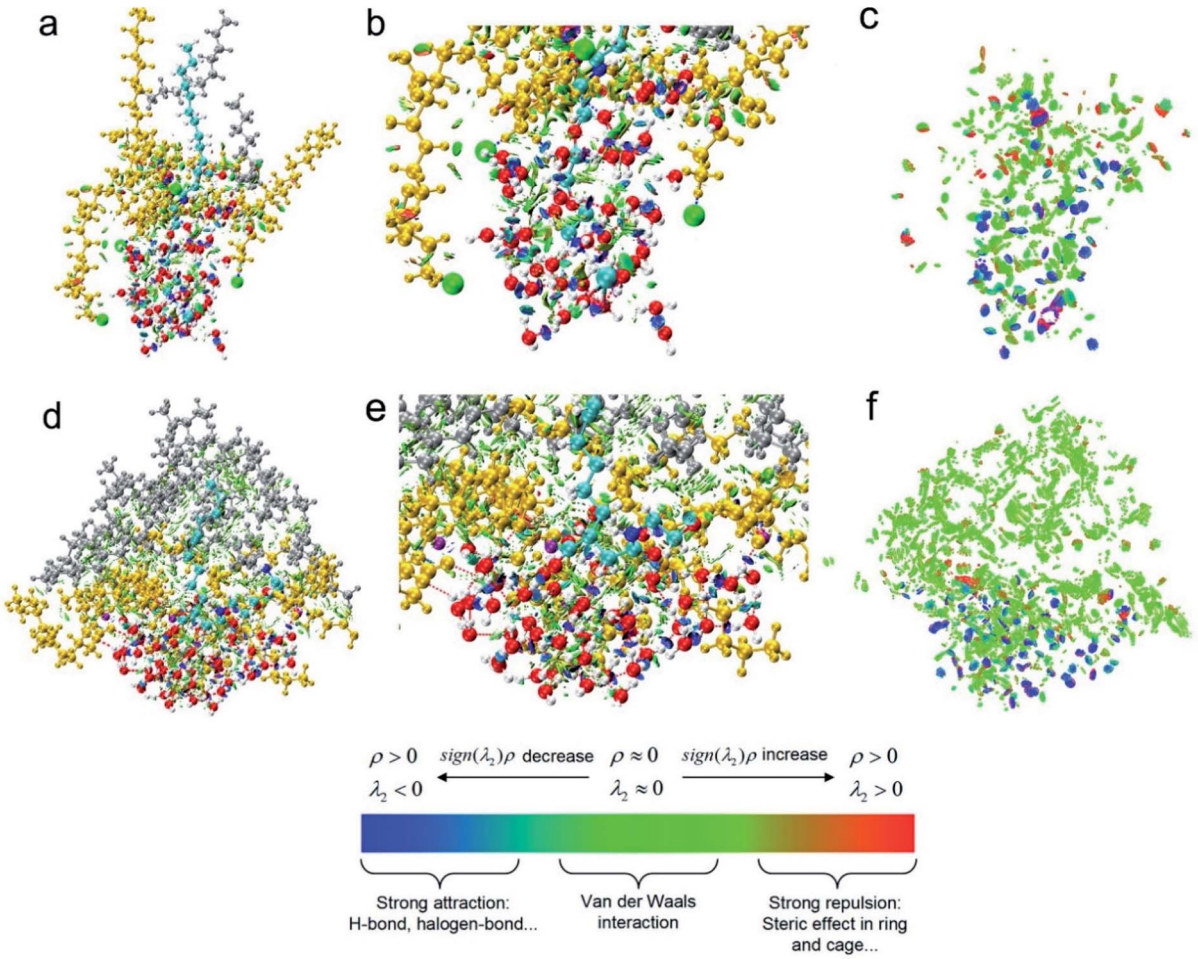

Fig. 9 RDG analysis of weak interaction: (a) **CTEA·HCl**, (b) magnification of weak interactions of **CTEA·HCl** (c) only indicate the distribution of **CTEA·HCl** weak interaction (d) **CTEA$^-$Na$^+$** (e) magnification of weak interactions of **CTEA$^-$Na$^+$** (f) only indicate the distribution of **CTEA$^-$Na$^+$** weak interaction. Cyan is the target surfactant molecule, gold is other surfactant molecules within 5 Å, gray is *n*-decane molecule, and red is water molecule. Weak effect in the color bar: red plate is repulsion interactions, blue plate is electrostatic interaction (mainly H-bonding interactions), and green plate is dispersion attraction (mainly van der Waals interactions).[7d,17]

Table 3 System information for simulation model

System	N_{sur}[a]	A_s[b] (nm^2 per sur)
Water/*n*-decane	0	—
CTHA·HCl	31	0.81
CTHA$^-$Na$^+$	25	1.00
CTEA·HCl	34	0.73
CTEA$^-$Na$^+$	27	0.92

[a] Surfactant number per interface N_{sur}. [b] Area per surfactant A_s.

100 kJ mol^{-1} nm^{-1}. At 298 K, an equilibration run of 1 ns was performed at an external pressure of 1 bar along the *z*-axis, which was perpendicular to the interface. The simulation time was extended to 5 ns, and the trajectories were kept every 1 ps.

Simulation method

All simulations in the current work were performed with the GROMACS 2020.3 MD simulation package.[20] The equations of motion were integrated with the leapfrog algorithm with a time step of 1.0 fs. The temperature was controlled by a v-rescale thermostat[21] and the pressure was controlled using the Berendsen barostat.[22] The (SPC/E) rigid water mode[23] and the GROMOS 54A7 united-atom force field[24] were used. The rigid structure of the water molecule was maintained using the Settle method,[25] and the bond lengths of all other molecules were constraint with the LINCS algorithm.[26] A cutoff of 0.9 nm was employed to calculate the short-range dispersion interactions, and the long-range dispersion corrections were also implemented for both energy and pressure. The long-range electrostatics were handled using the particle mesh Ewald (PME) method.[27] The trajectories were visualized by VMD software (version 1.9.3).[28]

Wavefunction analysis

Electrostatic potential distribution. The geometry of surfactant molecules was optimized by Gaussian 16 Rev. A.03 program[29] in gas (vacuum) environment at M06-2X/def-TZVP

level, and then the wavefunction was obtained. The electrostatic potential was calculated by cubegen of Multiwfn[30] version 3.6 code. VMD 1.9.3 program was employed to draw some isosurface maps of the cube file exported by Multiwfn to obtain better graphics.

Weak interactions. Optimization were completed by xtb program[31] at GFN2-xTB[32] level. After convergence, wavefunction at B3LYP/6-31G* level and RDG function[33] were analyzed through the Multiwfn program.[30] The isosurface shows weak interaction regions.

Conclusions

Understanding the effect of surfactant structure on their ability to modify interfacial properties is of great scientific and industrial interest. In this work, we have synthesized four ionic surfactants, including **CTHA·HCl**, **CTEA·HCl**, **CTHA$^-$Na$^+$** and **CTEA$^-$Na$^+$**. They differed in position of hydrophobic heads and component of hydrophobic tails. Experiment identified **CTEA$^-$Na$^+$** has the lowest interfacial tension. MD simulations shown that when the cationic hydrophilic group located in the proximal position, the molecule was relatively stretched. However, the geometry changed to a bending shape and the head-tail distance was greatly shorted when the anionic hydrophilic group was in the middle of the molecular. The DFT study and wavefunction analysis provide more fundamental information from weak interaction respect, which have shown that the **CTEA$^-$Na$^+$** could form a stronger vdW interactions with *n*-decane molecules. Moreover, introduction of polyethylene oxide groups made **CTEA$^-$Na$^+$** form a concentrated H-bonding network with water molecules on the interface. These differences in weak interactions may mainly contribute the conformational change of surfactants, which finally affected the properties of the interface.

In summary, the weak interactions and configuration of the surfactant molecules at the interface has a significant impact on its monolayers' properties. The insights gained from this work may offer a new sight to understand the surfactant structure and their adsorption behavior and may help improve the design of surfactants. Future work will focus on exploring more diverse surfactant structures as oil displacement, emulsification, oil extraction and other applications.

Author contributions

Conceptualization: Z. Z., F. Y.; formal analysis: Y. P. H.; investigation: W. Z., M. Y. Z.; methodology: Y. P. H., F. Y.; resources: Y. P. H., F. Y.; supervision: S. Z.; validation: R. S.; visualization: W. Z., M. Y. Z., K. W.; writing: Y. P. H., F. Y.

Conflicts of interest

There are no conflicts to declare.

Acknowledgements

This research work is supported by National Natural Science Foundation of China (Grant No. 21978124) and Key R&D Projects in Liaoning Province (Grant No. 2019JH2/10100005).

Notes and references

1 (*a*) A. Erfani, J. Seaberg, C. P. Aichele and J. D. Ramsey, *Biomacromolecules*, 2020, **21**(7), 2557–2573; (*b*) W. Shinoda, R. DeVane and M. L. Klein, *J. Phys. Chem. B*, 2010, **114**(20), 6836–6849.

2 (*a*) D. Myers, *Surfactant Science and Technology*, VCH, New York, 1946; (*b*) K. Bouchemal, S. Briançon, E. Perrier and H. Fessi, *Int. J. Pharm.*, 2004, **280**, 241–251; (*c*) A. P. Gerola, P. F. A. Costa, F. H. Quina, H. D. Fiedler and F. Nome, *Curr. Opin. Colloid Interface Sci.*, 2017, **32**, 39–47; (*d*) E. Dickinson, S. R. Euston and C. M. Woskett, *Prog. Colloid Polym. Sci.*, 1990, **82**, 65–75; (*e*) X. Tian, Q. Fan, J. Guo, Q. Yu, L. Xu and X. Kong, *Spectrochim. Acta, Part A*, 2021, **263**, 120174; (*f*) M. M. Hassan and C. M. Carr, *Chemosphere*, 2021, **265**, 129087.

3 (*a*) O. Castellani, S. Al-Assaf, M. Axelos, G. O. Phillips and M. Anton, *Food Hydrocolloids*, 2010, **24**, 121–130; (*b*) S. Palchowdhury and B. L. Bhargava, *J. Mol. Liq.*, 2017, **234**, 249–259; (*c*) Z. Liu, L. Jiang, X. Fu, J. Zhang and J. Lei, *J. Therm. Anal. Calorim.*, 2020, **140**(5), 2159–2170; (*d*) H. Xiao, Z. Zhen, H. Sun, X. Cao, Z. Li, X. Song and X. Liu, *Sci. China: Chem.*, 2010, **53**(4), 945–949; (*e*) Q. Tao, Y. N. Li, W. J. Tang, P. Y. Liu, F. Yu and Y.-P. He, *Tetrahedron Lett.*, 2021, **74**, 153158; (*f*) Y. Yang, Z. Ma, F. Xia and X. Li, *J. Water Process. Eng.*, 2020, **36**, 101292; (*g*) G. Zhao, Z. Yuan, X. Liu, P. Wang, J. Yin and S. Ma, *J. Mol. Liq.*, 2020, **317**, 113980; (*h*) W. Sun, Q. Ren, Z. Wang and F. Yang, *Langmuir*, 2019, **35**, 911–920; (*i*) R. Wu, M. Deng, B. Kong, Y. Wang and X. Yang, *J. Phys. Chem. B*, 2009, **113**, 12680–12686.

4 (*a*) L. Zhang, Z. Liu, T. Ren, P. Wu, J. Shen, W. Zhang and X. Wang, *Langmuir*, 2014, **30**(46), 13815–13822; (*b*) H. Domínguez, *J. Phys. Chem. B*, 2011, **115**(43), 12422–12428; (*c*) K. J. Schweighofer, U. Essmann and M. Berkowitz, *J. Phys. Chem. B*, 1997, **101**(19), 3793–3799; (*d*) J. Kubelka, S. Bai and M. Piri, *J. Phys. Chem. B*, 2021, **125**(4), 1293–1305; (*e*) C. V. Nguyen, T. V. Nguyen and C. M. Phan, *Int. J. Heat Mass Transfer*, 2017, **106**, 1035–1040; (*f*) J. Ma, X. Song, j. Luo, T. Zhao, H. Yu, B. Peng and S. Zhao, *Langmuir*, 2019, **35**(42), 13636–13645.

5 (*a*) G. Rucker, X. Yu and L. Zhang, *Fuel*, 2020, **267**, 117252; (*b*) Y. Hu, J. Han and R. Guo, *Langmuir*, 2020, **36**(35), 10494–10503; (*c*) K. A. Becraft and G. L. Richmond, *J. Phys. Chem. B*, 2005, **109**(11), 5108–5117; (*d*) M. Wang, T. Fang, P. Wang, X. Tang, B. Sun, J. Zhang and B. Liu, *Soft Matter*, 2016, **12**, 8177–8185; (*e*) C. Hill, Y. Umetsu, K. Fujita, T. Endo, K. Sato, A. Yoshizawa, S. E. Rogers, J. Eastoe and M. Sagisaka, *Langmuir*, 2020, **36**(48), 14829–14840; (*f*) R. Sun, K. Hong, Z. Lv, X. Ding and F. Yu, *J. Surfactants Deterg.*, 2018, **21**(4), 461–466.

6 (*a*) W. Wang, W. Lu and L. Jiang, *J. Phys. Chem. B*, 2008, **112**(5), 1409–1413; (*b*) F. Tu and D. Lee, *J. Am. Chem. Soc.*, 2014, **136**(28), 9999–10006; (*c*) X. Li, Y. Yang, J. Eastoe and J. Dong, *ChemPhysChem*, 2010, **11**, 3074–3077; (*d*) J. Lee, Z. Zhou and S. H. Behrens, *J. Phys. Chem. B*, 2015, **119**(22), 6628–6637; (*e*) J. Hu, C. Sanders, S. Mekala, T.-Y. Chen, M. F. Cunningham and R. A. Gross, *Macromolecules*, 2019, **52**, 1517–1525.

7 (*a*) H. Tao, C. Lian and H. Liu, *Green Energy Environ.*, 2020, **5**, 303–321; (*b*) T. Su, K. Hong, W. Zhang, F. Li, Q. Li, F. Yu, G. Luo, H. Gao and Y.-P. He, *Soft Matter*, 2017, **13**(22), 4066–4073; (*c*) Z. Shen, Y. Jiang, T. Wang and M. Liu, *J. Am. Chem. Soc.*, 2015, **137**, 16109–16115; (*d*) W. Zhang, Z. Zhang, S. Zhao, K. Hong, M. Zhang, L. Song, F. Yu, G. Luo and Y.-P. He, *Langmuir*, 2021, **37**(9), 2954–2962.

8 C. Xue, G. Qu, Y. Han, S. Li, X. Gao and W. Ding, *J. Dispersion Sci. Technol.*, 2016, **37**, 1480–1485.

9 Y. Wei, G. Liu, Z. Wang and S. Yuan, *RSC Adv.*, 2016, **6**, 49708–49716.

10 (*a*) F. Eisenhaber, P. Lijnzaad, P. Argos, C. Sander and M. Scharf, *J. Comput. Chem.*, 1995, **16**(3), 273–284; (*b*) Y. Zhao and D. G. Truhlar, *Theor. Chem. Acc.*, 2008, **120**, 215–241.

11 J. G. Kirkwood and F. P. Buff, *J. Chem. Phys.*, 1949, **17**, 338–343.

12 D. M. Mitrinović, A. M. Tikhonov, M. Li, Z. Huang and M. L. Schlossman, *Phys. Rev. Lett.*, 2000, **85**(3), 582.

13 (*a*) E. Calvo, P. Brocos, R. Bravo, M. Pintos, A. Amigo, A. H. Roux and G. Roux-Desgranges, *J. Chem. Eng. Data*, 1998, **43**(1), 105–111; (*b*) N. V. Sastry and M. K. Valand, *J. Chem. Thermodyn.*, 1998, **30**(8), 929–938; (*c*) J. L. Trenzado, J. S. Matos, L. Segade and E. Carballo, *J. Chem. Eng. Data*, 2001, **46**(4), 974–983; (*d*) B. S. Bjola, M. A. Siddiqi, U. Fornefeld-Schwarz and P. Svejda, *J. Chem. Eng. Data*, 2002, **47**(2), 250–253.

14 (*a*) N. G. Tsierkezos and I. E. Molinou, *J. Chem. Eng. Data*, 1998, **43**(6), 989–993; (*b*) Y. Pai and L. Chen, *J. Chem. Eng. Data*, 1998, **43**(4), 665–667.

15 S. S. Jang, S. Lin, P. K. Maiti, M. Blanco, W. A. Goddard, P. Shuler and Y. Tang, *J. Phys. Chem. B*, 2004, **108**(32), 12130–12140.

16 R. Kumar, J. R. Schmidt and J. L. Skinner, *J. Chem. Phys.*, 2007, **126**, 204107.

17 (*a*) T. Luand and Q. Chen, *J. Mol. Model.*, 2020, **26**(11), 1–9; (*b*) S. Emamian, T. Lu, H. Kruse and H. Emamian, *J. Comput. Chem.*, 2019, **40**, 2868–2881.

18 M. Stroet, B. Caron, K. M. Visscher, D. P. Geerke, A. K. Malde and A. E. Mark, *J. Chem. Theory Comput.*, 2018, **14**(11), 5834–5845.

19 (*a*) J. M. Martínez and L. Martínez, *J. Comput. Chem.*, 2003, **24**, 819–825; (*b*) L. Martínez, R. Andrade, E. G. Birgin and J. M. Martínez, *J. Comput. Chem.*, 2009, **30**, 2157–2164.

20 E. Lindahl, M. Abraham, B. Hess and D. Van Der Spoel, *GROMACS 2020.3 Source code (Version 2020.3)*, 2020.

21 G. Bussi, D. Donadio and M. Parrinello, *J. Chem. Phys.*, 2007, **126**, 014101.

22 H. J. C. Berendsen, J. P. M. Postma, W. F. Van Gunsteren, A. DiNola and J. R. Haak, *J. Chem. Phys.*, 1984, **81**, 3684–3690.

23 H. J. C. Berendsen, J. R. Grigera and T. P. Straatsma, *J. Phys. Chem.*, 1987, **91**(24), 6269–6271.

24 (*a*) N. Schmid, A. P. Eichenberger and A. Choutko, *Eur. Biophys. J.*, 2011, **40**, 843–856; (*b*) W. Huang, Z. Lin and W. F. Gunsteren, *J. Chem. Theory Comput.*, 2011, **7**(5), 1237–1243.

25 S. Miyamoto and P. A. Kollman, *J. Comput. Chem.*, 1992, **13**(8), 952–962.

26 B. Hess, H. Bekker, H. J. C. Berendsen and J. G. E. M. Fraaije, *J. Comput. Chem.*, 1997, **18**(12), 1463–1472.

27 T. Darden, D. York and L. Pedersen, *J. Chem. Phys.*, 1993, **98**(12), 10089–10092.

28 W. Humphrey, A. Dalke and K. Schulten, *J. Mol. Graphics*, 1996, **14**(1), 33–38.

29 M. J. Frisch, G. W. Trucks, H. B. Schlegel, G. E. Scuseria, M. A. Robb, J. R. Cheeseman, G. Scalmani, V. Barone, G. A. Petersson, H. Nakatsuji, X. Li, M. Caricato, A. V. Marenich, J. Bloino, B. G. Janesko, R. Gomperts, B. Mennucci, H. P. Hratchian, J. V. Ortiz, A. F. Izmaylov, J. L. Sonnenberg, D. Williams-Young, F. Ding, F. Lipparini, F. Egidi, J. Goings, B. Peng, A. Petrone, T. Henderson, D. Ranasinghe, V. G. Zakrzewski, J. Gao, N. Rega, G. Zheng, W. Liang, M. Hada, M. Ehara, K. Toyota, R. Fukuda, J. Hasegawa, M. Ishida, T. Nakajima, Y. Honda, O. Kitao, H. Nakai, T. Vreven, K. Throssell, J. A. Montgomery Jr, J. E. Peralta, F. Ogliaro, M. J. Bearpark, J. J. Heyd, E. N. Brothers, K. N. Kudin, V. N. Staroverov, T. A. Keith, R. Kobayashi, J. Normand, K. Raghavachari, A. P. Rendell, J. C. Burant, S. S. Iyengar, J. Tomasi, M. Cossi, J. M. Millam, M. Klene, C. Adamo, R. Cammi, J. W. Ochterski, R. L. Martin, K. Morokuma, O. Farkas, J. B. Foresman and D. J. Fox, *Gaussian 16, Revision A.03*, Gaussian, Inc., Wallingford CT, 2016.

30 (*a*) T. Lu and F. Chen, *J. Comput. Chem.*, 2012, **33**, 580–592; (*b*) G. Chen, P.-Y. Liu, H. Zou, J. Hu, X. Fang, D. Xu, Y.-P. He, H. Wei and W. Xie, *Org. Lett.*, 2021, **23**, 2279–2284; (*c*) Q. Tao, Y.-N. Li, W.-J. Tang, P.-Y. Liu, F. Yu and Y.-P. He, *Tetrahedron Lett.*, 2021, **74**, 153158.

31 (*a*) C. Bannwarth, E. Caldeweyher and S. Grimme, *Wiley Interdiscip. Rev.: Comput. Mol. Sci.*, 2020, **11**, e01493; (*b*) P.-P. Niu, P.-Y. Liu, Y.-N. Meng, F. Yu and Y.-P. He, *J. Org. Chem.*, 2021, **86**, 3096–3106.

32 C. Bannwarth, S. Ehlert and S. Grimme, *J. Chem. Theory Comput.*, 2019, **15**(3), 1652–1671.

33 E. R. Johnson, S. Keinan, P. Mori-Sánchez, J. Contreras-García, A. J. Cohen and W. Yang, *J. Am. Chem. Soc.*, 2010, **132**, 6498–6506.